

The CP properties of the lightest Higgs boson with sbottom effects

Müge Boz

Hacettepe University, Department of Physics,
06532 Ankara, Turkey

ABSTRACT

In the framework of the recently proposed gluino-axion model, using the effective potential method and taking into account the top-stop as well as the bottom-sbottom effects, we discuss the CP-properties of the lightest Higgs boson, in particular its CP-odd composition, which can offer new opportunities at collider searches. It is found that although the CP-odd composition of the lightest Higgs increases slightly with the inclusion of the sbottom effects, it never exceeds %0.17 for all values of the renormalization scale Q ranging from top mass to TeV scale

1 Introduction

The radiative corrections to the masses of Higgs bosons in the MSSM have received much attention from the beginning, and an important step in the understanding of the MSSM Higgs sector was the significant modification of the tree level bound by the radiative corrections, dominated by the top quark and top squark loops [1, 2, 3, 4]. The radiative corrections have been computed by using different approximations such as the effective potential [2, 3, 4], and diagrammatic [1, 5] methods. More complete treatment of these results include the complete one-loop on-shell renormalization [6], the renormalization group (RG) improvement for resumming the leading logarithms [7, 8, 9], the iteration of the RG equations to two-loops with the use of the effective potential techniques [10, 11, 12, 13] and two loop on-shell renormalization [14, 15, 16].

In the recent literature, the studies on the radiatively induced CP violation effects and the theoretical predictions for the Higgs boson masses and couplings as functions of relevant minimal SUSY model(MSSM) parameters has been carried out in several directions. For example, in [17, 18], the implications of the presence of CP phases in the soft SUSY breaking sector allowing to the mixing of CP even and CP odd states were discussed. More recently the mass matrix of the neutral Higgs bosons of the MSSM has been calculated using the effective potential method, in the case of the small splittings between squark mass eigenstates in [19], taking into account only the dominant top-stop contributions in [20] and including the sbottom contributions in [21]. Additional contributions from the chargino, W and the charged Higgs exchange loops were computed in [22]. In [23], one-loop corrections to the mass matrix of the neutral Higgs bosons in the MSSM were calculated by using the effective potential method for an arbitrary splitting between squark masses, including the electroweak and gauge couplings and the leading two loop corrections. More complete treatment of the effective Higgs potential in the MSSM including the two-loop leading logarithms induced by top-bottom Yukawa couplings as well as those associated with QCD corrections by means of RG methods were performed in [24].

It is a well-known fact that in the supersymmetric (SUSY) extensions of S.M, apart from the physical phases δ_{CKM} and θ_{QCD} , also existing in the SM, there appear novel sources of CP violation via the phases of the soft supersymmetry breaking mass terms [25]. Besides their contribution to the known CP-violating observables such as electric dipole moments of the particles [26, 27], these phases also induce CP violation in the Higgs sector [17, 18, 19, 20, 28, 29]. Moreover, the SUSY theories which are designed to solve the hierarchy problems, possess two hierarchy problems: One concerning the strong CP problem, also existing in the S.M, whose source is the neutron EDM exceeding the present bounds by nine orders of magnitude [30] and the other is the μ puzzle, concerning the Higgsino Dirac mass parameter μ which follows from

the superpotential of the model. A simultaneous solution to these two hierarchy problems can be achieved by the gluino-axion model[31, 32, 33] with a new kind of axion [34, 35, 36, 37], which couples to the gluino rather than to quarks. Besides, the low energy theory is identical to the MSSM with all sources of the soft SUSY phases. Due to all these abilities of the model, in the analysis below we shall adopt its parameter space.

In the recent literature, the radiative corrections to the Higgs masses and mixings, dominated by the top-stop contributions have been studied in gluino-axion model [39]. In Ref. [39], which was based on Ref. [20], the mass squared matrix of Higgs scalars involves the one loop function $g(x, y)$, as well as the other scale-independent terms. The function $g(x, y)$ is related to $f(x, y)$ in such a way that $g(x, y) = f(x, y) - \log \frac{xy}{Q^4}$, where $f(x, y)$ is a scale-dependent loop function whose expression is given by $f(x, y) = -2 + \log \frac{xy}{Q^4} + \frac{y+x}{y-x} \log \frac{y}{x}$. However, since the explicit dependence of Q in the one-loop function $f(x, y)$ is actually cancelled by the explicit Q dependence of the function $g(x, y)$, then, $g(x, y) = -2 + \frac{y+x}{y-x} \log \frac{y}{x}$ does not have an explicit dependence on the renormalization scale Q , unlike $f(x, y)$. Therefore, in both of the works of [20, 39] the elements of the mass squared matrix of Higgs scalars, which depend only on the scale-independent function $g(x, y)$ as well as the other scale-independent terms, do not have an explicit dependence on Q . Actually, in [20, 39] the one-loop bottom-sbottom contributions to ΔV are not included, and the terms proportional to μ , A_t are obtained by neglecting the D-terms in the stop masses, to gain independence of the renormalization scale Q , since the D-term contributions to the squark masses are quite small. On the other hand, in Ref. [21] the one-loop bottom sbottom contributions as well as the top-stop contributions to radiative corrections are taken into consideration. Thus, the elements of the mass squared mass matrix of the Higgs scalars not only include the scale-independent function $g(x, y)$ with various parameters, but have an explicit dependence on the renormalization scale through the scale dependent function $f(x, y)$, and the scale dependent logarithmic terms, stemming from the additional contributions to the radiative corrections.

The main purpose of this work is to analyze the CP violation effects on the lightest Higgs boson in the framework of the gluino-axion model using the recent experimental data [38], by the inclusion of the bottom-sbottom effects, as well as the top- stop contributions. As the Q -dependence is taken into consideration, we particularly adress the issues, whether or not the various renormalization scales, all being around the weak scale, would lead us to a large amount of CP violation opportunities, and, investigate whether one can find an appropriate limit of reasonable agreement with the scale-independent results [39]. We will base our calculations to those of Ref. [21], However, we differ from [21] in the sense that in our analysis, all the chosen parameters are specific to the gluino-axion model, namely all the soft mass parameters in this theory are fixed in terms of the μ parameter.

The organization of this work is as follows: In Sec. 2, starting from the Higgs sector structure of the gluino-axion model, we compute the (3×3) dimensional mass matrix of the Higgs scalars whose elements are expressed in terms of the parameters of the model under concern. In Sec. 3, we make the numerical analysis to study the CP violation effects on the lightest Higgs boson, and analyze the influence of Q on its CP-odd composition, as well as on μ . We conclude in Sec. 4.

2 The model

In the gluino-axion model, the invariance of the supersymmetric Lagrangian and the invariance of all supersymmetry breaking terms under $U(1)_R$ are guaranteed by promoting the ordinary μ operator to a composite operator containing the singlet composite superfield \hat{S} with unit R charge [31]. When the scalar component of the singlet develops a vacuum expectation value around the Peccei-Quinn scale $v_s \sim 10^{11}$ GeV, an effective μ -parameter \sim a TeV is induced such that

$$\mu \equiv v_s^2/M_{Pl} \times e^{-i\theta_{QCD}/3} \sim \text{a TeV} \times e^{-i\theta_{QCD}/3} \quad (1)$$

where θ_{QCD} is the effective QCD vacuum angle. Therefore, the vacuum expectation value of the singlet serves for two important purposes for the model under concern: Its magnitude determines the scale of supersymmetry breaking and its phase solves the strong CP-problem.

The effective Lagrangian at low-energy is given by [31]:

$$\begin{aligned} \mathcal{L}_{MSSM}^{soft} = & \tilde{Q}^\dagger M_Q^2 \tilde{Q} + \tilde{u}^{c\dagger} M_{u^c}^2 \tilde{u}^c + \tilde{d}^{c\dagger} M_{d^c}^2 \tilde{d}^c + \tilde{L}^\dagger M_L^2 \tilde{L} + \tilde{e}^{c\dagger} M_{e^c}^2 \tilde{e}^c \\ & + \left\{ A_u \tilde{Q} \cdot H_u \tilde{u}^c + A_d \tilde{Q} \cdot H_d \tilde{d}^c + A_e \tilde{L} \cdot H_d \tilde{e}^c \right\} + h.c. \\ & + M_{H_u}^2 |H_u|^2 + M_{H_d}^2 |H_d|^2 + (\mu B H_u \cdot H_d + h.c.) \\ & + \left\{ M_3 \tilde{\lambda}_3^a \tilde{\lambda}_3^a + M_2 \tilde{\lambda}_2^i \tilde{\lambda}_2^i + M_1 \tilde{\lambda}_1 \tilde{\lambda}_1 + h.c. \right\}, \end{aligned} \quad (2)$$

The soft terms of the low energy Lagrangian in the gluino-axion model are identical to those in the general MSSM except for the fact that the soft masses are all expressed in terms of the μ parameter through appropriate flavour matrices except for the fact that the soft masses are all expressed in terms of the μ parameter through appropriate flavour matrices. The flavour matrices form the sources of CP violation and intergenerational mixings in the squark sector. The phases of the trilinear couplings $(A_{u,d,e})$, the gaugino masses $(M_{3,2,1})$, and the effective μ -parameter defined in (1) are the only phases which can generate CP violation observables.

It is known that the dominant contributions to the one-loop radiative corrections come from the the top quark and top squark loops as long as $\tan \beta \lesssim 50$, as in the CP-conserving case [1, 2, 3, 4]. However, for a more sensitive calculation, we will take into account of the

contributions from the bottom- sbottom, as well as the top-stop quark loops. For convenience, we set the soft SUSY breaking scalar-quark masses as $M_{\tilde{Q}} = M_{\tilde{u}} = M_{\tilde{d}}$, and the squark trilinear couplings as $A_t = A_b$. Then, the explicit expressions for the mass parameters in (2) defined as follows: The top (bottom) squark soft masses are given by:

$$M_{\tilde{Q}}^2 = k_Q^2 |\mu|^2, \quad (3)$$

where k_Q is a real parameter. The top(bottom) squark trilinear couplings read as:

$$A_t = \mu k_t^*, \quad (4)$$

where k_t is a complex parameter. The tree level Higgs soft masses are defined by:

$$M_{H_u}^2 = y_u |\mu|^2, \quad M_{H_d}^2 = y_d |\mu|^2, \quad \mu B = |\mu|^2 \left(\frac{8m_s^2}{v_s^2} + k_\mu \right), \quad (5)$$

where $m_s^2 \sim v_s^2$ is a natural choice as discussed in [31]. Here y_u and y_d are real parameters, and k_μ is a complex parameter determining the phase of the B parameter. which can be identified with the relative phase of the Higgs doublets [20].

After electroweak breaking the Higgs doublets in (2) can be expanded as

$$\begin{aligned} H_d &= \begin{pmatrix} H_d^0 \\ H_d^- \end{pmatrix} = \frac{1}{\sqrt{2}} \begin{pmatrix} v_d + \phi_1 + i\varphi_1 \\ H_d^- \end{pmatrix}, \\ H_u &= \begin{pmatrix} H_u^+ \\ H_u^0 \end{pmatrix} = \frac{e^{i\theta}}{\sqrt{2}} \begin{pmatrix} H_u^+ \\ v_u + \phi_2 + i\varphi_2 \end{pmatrix}. \end{aligned} \quad (6)$$

where $\tan \beta \equiv v_u/v_d$ as usual, and the angle parameter θ is the misalignment between the two Higgs doublets.

We follow the effective potential method for computing the one-loop corrected Higgs masses and mixings. As usual, the entries of the Higgs masses and their mixings can be calculated up to one loop accuracy by the second derivatives of the effective potential with respect to the Higgs fields.

$$M^2 = \left(\frac{\partial^2 V}{\partial \chi_i \partial \chi_j} \right)_0, \text{ where } \chi_i \in \mathcal{B} = \{\phi_1, \phi_2, \varphi_1, \varphi_2\}, \quad (7)$$

where $V \equiv V_0 + V_{1-loop}$ is the radiatively corrected Higgs potential [21], and as we mentioned before we take into account the top-stop and bottom-sbottom loop corrections. The stop and sbottom mass-squared eigenvalues are given by:

$$m_{t_{1,2}}^2 = \frac{1}{4} M_Z^2 c_{2\beta} + m_t^2 + k_Q^2 |\mu|^2 \mp \Delta_t^2, \quad (8)$$

$$m_{b_{1,2}}^2 = -\frac{1}{4}M_Z^2 c_{2\beta} + m_b^2 + k_Q^2 |\mu|^2 \mp \Delta_b^2, \quad (9)$$

with,

$$\Delta_t^2 = \sqrt{\left(\frac{2}{3}M_W^2 - \frac{5}{12}M_Z^2\right)^2 c_{2\beta}^2 + m_t^2 |\mu|^2 \left(|k_t|^2 + t_\beta^{-2} - 2|k_t|t_\beta^{-1} c_{\varphi_{kt}}\right)}, \quad (10)$$

$$\Delta_b^2 = \sqrt{\left(\frac{1}{12}M_Z^2 - \frac{1}{3}M_W^2\right)^2 c_{2\beta}^2 + m_b^2 |\mu|^2 \left(|k_t|^2 + t_\beta^2 - 2|k_t|t_\beta c_{\varphi_{kt}}\right)}, \quad (11)$$

where $c_\beta = \cos \beta$, $c_{\varphi_{kt}} = \cos \varphi_{kt}$, $s_\beta = \sin \beta$, $s_{\varphi_{kt}} = \sin \varphi_{kt}$, $t_\beta = \tan \beta$, $t_\beta^{-1} = \cot \beta$. The stop and sbottom mass splittings depend explicitly on the total CP violation angle φ_{kt} such that

$$\varphi_{kt} = \text{Arg}[\mu A_t^*] = \text{Arg}[k_t], \quad (12)$$

where k_t has been defined in (4).

The (3×3) dimensional Higgs mass-squared matrix can be expressed as:

$$\begin{pmatrix} M_Z^2 c_\beta^2 + \tilde{M}_A^2 s_\beta^2 + \Delta_{11} & -(M_Z^2 + \tilde{M}_A^2) s_\beta c_\beta + \Delta_{12} & \Delta_{13} \\ -(M_Z^2 + \tilde{M}_A^2) s_\beta c_\beta + \Delta_{12} & M_Z^2 s_\beta^2 + \tilde{M}_A^2 c_\beta^2 + \Delta_{22} & \Delta_{23} \\ \Delta_{13} & \Delta_{23} & \tilde{M}_A^2 + \Delta_{33} \end{pmatrix} \quad (13)$$

in the basis $\mathcal{B} = \{\phi_1, \phi_2, \sin \beta \varphi_1 + \cos \beta \varphi_2\}$ using (6).

The elements of the radiatively corrected mass-squared matrix read as:

$$\begin{aligned} \Delta_{11t} &= \frac{\beta_k}{2} \left[\frac{M_Z^4 c_\beta^2}{8} \log \frac{m_{t_2}^2 m_{t_1}^2}{Q^4} + \frac{M_Z^2 c_\beta}{2} \frac{(2m_t^2 \mu \mathcal{R}_{t1} + \frac{1}{2} s_{2\beta} \mathcal{X}_t)}{s_\beta (m_{t_2}^2 - m_{t_1}^2)} \log \frac{m_{t_2}^2}{m_{t_1}^2} \right. \\ &\quad - \frac{1}{2} \left(\frac{2k_t m_t^2 \mu^2 c_{\varphi_{kt}}}{s_{2\beta}} - \mathcal{Z}_t(M_W, M_Z) c_\beta^2 \right) f(m_{t_1}^2, m_{t_2}^2) \\ &\quad \left. - \frac{(2m_t^2 \mu \mathcal{R}_{t1} + \frac{1}{2} s_{2\beta} \mathcal{X}_t)^2}{2s_\beta^2 (m_{t_2}^2 - m_{t_1}^2)^2} g(m_{t_1}^2, m_{t_2}^2) \right] \end{aligned} \quad (14)$$

$$\begin{aligned} \Delta_{11b} &= \frac{\beta_k}{2} \left[-\frac{4m_b^4}{c_\beta^2} \log \frac{m_b^2}{Q^2} + \frac{1}{2} \left(\frac{2m_b^2}{c_\beta} - \frac{M_Z^2 c_\beta}{2} \right)^2 \log \frac{m_{b_2}^2 m_{b_1}^2}{Q^4} \right. \\ &\quad + \frac{1}{2} \left(\frac{4m_b^2}{c_\beta} - M_Z^2 c_\beta \right) \frac{(2k_t m_b^2 \mu \mathcal{R}_{b2} - c_\beta^2 \mathcal{X}_b)}{c_\beta (m_{b_2}^2 - m_{b_1}^2)} \log \frac{m_{b_2}^2}{m_{b_1}^2} \\ &\quad - \frac{1}{2} \left(\frac{k_t m_b^2 \mu^2 t_\beta c_{\varphi_{kt}}}{c_\beta^2} - \mathcal{Z}_b(M_W, M_Z) c_\beta^2 \right) f(m_{b_1}^2, m_{b_2}^2) \\ &\quad \left. - \frac{(2k_t m_b^2 \mu \mathcal{R}_{b2} - c_\beta^2 \mathcal{X}_b)^2}{2c_\beta^2 (m_{b_2}^2 - m_{b_1}^2)^2} g(m_{b_1}^2, m_{b_2}^2) \right]. \end{aligned} \quad (15)$$

$$\begin{aligned}
\Delta_{22t} = & \frac{\beta_k}{2} \left[-\frac{4m_t^4}{s_\beta^2} \log \frac{m_t^2}{Q^2} + \frac{1}{2} \left(\frac{2m_t^2}{s_\beta} - \frac{M_Z^2 s_\beta}{2} \right)^2 \log \frac{m_{\tilde{t}_2}^2 m_{\tilde{t}_1}^2}{Q^4} \right. \\
& + \frac{1}{2} \left(\frac{4m_t^2}{s_\beta} - M_Z^2 s_\beta \right) \frac{(2k_t m_t^2 \mu \mathcal{R}_{t2} - s_\beta^2 \mathcal{X}_t)}{s_\beta (m_{\tilde{t}_2}^2 - m_{\tilde{t}_1}^2)} \log \frac{m_{\tilde{t}_2}^2}{m_{\tilde{t}_1}^2} \\
& - \frac{1}{2} \left(\frac{k_t m_t^2 \mu^2 t_\beta^{-1} c_{\varphi_{kt}}}{s_\beta^2} - \mathcal{Z}_t(M_W, M_Z) s_\beta^2 \right) f(m_{\tilde{t}_1}^2, m_{\tilde{t}_2}^2) \\
& \left. - \frac{(2k_t m_t^2 \mu \mathcal{R}_{t2} - s_\beta^2 \mathcal{X}_t)^2}{2s_\beta^2 (m_{\tilde{t}_2}^2 - m_{\tilde{t}_1}^2)^2} g(m_{\tilde{t}_1}^2, m_{\tilde{t}_2}^2) \right]. \tag{16}
\end{aligned}$$

$$\begin{aligned}
\Delta_{22b} = & \frac{\beta_k}{2} \left[\frac{M_Z^4 s_\beta^2}{8} \log \frac{m_{\tilde{b}_2}^2 m_{\tilde{b}_1}^2}{Q^4} + \frac{M_Z^2 c_\beta}{2} \frac{(2m_b^2 \mu \mathcal{R}_{b1} + \frac{1}{2} s_{2\beta} \mathcal{X}_b)}{c_\beta (m_{\tilde{b}_2}^2 - m_{\tilde{b}_1}^2)} \log \frac{m_{\tilde{b}_2}^2}{m_{\tilde{b}_1}^2} \right. \\
& - \frac{1}{2} \left(\frac{2k_t m_b^2 \mu^2 c_{\varphi_{kt}}}{s_{2\beta}} - \mathcal{Z}_b(M_W, M_Z) s_\beta^2 \right) f(m_{\tilde{b}_1}^2, m_{\tilde{b}_2}^2) \\
& \left. - \frac{(2m_b^2 \mu \mathcal{R}_{b1} + \frac{1}{2} s_{2\beta} \mathcal{X}_b)^2}{2c_\beta^2 (m_{\tilde{b}_2}^2 - m_{\tilde{b}_1}^2)^2} g(m_{\tilde{b}_1}^2, m_{\tilde{b}_2}^2) \right] \tag{17}
\end{aligned}$$

$$\Delta_{33t} = \frac{\beta_k}{2} \left[-\frac{2k_t^2 m_t^4 \mu^4 s_{\varphi_{kt}}^2}{s_\beta^4 (m_{\tilde{t}_2}^2 - m_{\tilde{t}_1}^2)^2} g(m_{\tilde{t}_1}^2, m_{\tilde{t}_2}^2) - \frac{1}{2} \frac{k_t m_t^2 \mu^2 c_{\varphi_{kt}}}{s_\beta^3 c_\beta} f(m_{\tilde{t}_1}^2, m_{\tilde{t}_2}^2) \right] \tag{18}$$

$$\Delta_{33b} = \frac{\beta_k}{2} \left[-\frac{2k_t^2 m_b^4 \mu^4 s_{\varphi_{kt}}^2}{c_\beta^4 (m_{\tilde{b}_2}^2 - m_{\tilde{b}_1}^2)^2} g(m_{\tilde{b}_1}^2, m_{\tilde{b}_2}^2) - \frac{1}{2} \frac{k_t m_b^2 \mu^2 c_{\varphi_{kt}}}{c_\beta^3 s_\beta} f(m_{\tilde{b}_1}^2, m_{\tilde{b}_2}^2) \right] \tag{19}$$

$$\begin{aligned}
\Delta_{12t} = & \frac{\beta_k}{2} \left[\frac{M_Z^2 s_{2\beta}}{16} \left(\frac{4m_t^2}{s_\beta^2} - M_Z^2 \right) \log \frac{m_{\tilde{t}_2}^2 m_{\tilde{t}_1}^2}{Q^4} \right. \\
& + \frac{M_Z^2 c_\beta}{4} \frac{(2k_t m_t^2 \mu \mathcal{R}_{t2} - s_\beta^2 \mathcal{X}_t)}{s_\beta (m_{\tilde{t}_2}^2 - m_{\tilde{t}_1}^2)} \log \frac{m_{\tilde{t}_2}^2}{m_{\tilde{t}_1}^2} + \\
& + \frac{1}{4} \left(\frac{4m_t^2}{s_\beta} - M_Z^2 s_\beta \right) \frac{(2m_t^2 \mu \mathcal{R}_{t1} + \frac{1}{2} s_{2\beta} \mathcal{X}_t)}{s_\beta (m_{\tilde{t}_2}^2 - m_{\tilde{t}_1}^2)} \log \frac{m_{\tilde{t}_2}^2}{m_{\tilde{t}_1}^2} \\
& + \frac{1}{4} \left(\frac{2k_t m_t^2 \mu^2 c_{\varphi_{kt}}}{s_\beta^2} - \frac{1}{2} \mathcal{Z}_t(M_W, M_Z) s_{2\beta} \right) f(m_{\tilde{t}_1}^2, m_{\tilde{t}_2}^2) \\
& \left. - \frac{(2m_t^2 \mu \mathcal{R}_{t1} + \frac{1}{2} s_{2\beta} \mathcal{X}_t)(2k_t m_t^2 \mu \mathcal{R}_{t2} - s_\beta^2 \mathcal{X}_t)}{2s_\beta^2 (m_{\tilde{t}_2}^2 - m_{\tilde{t}_1}^2)^2} g(m_{\tilde{t}_1}^2, m_{\tilde{t}_2}^2) \right] \tag{20}
\end{aligned}$$

$$\Delta_{12b} = \frac{\beta_k}{2} \left[\frac{M_Z^2 s_{2\beta}}{16} \left(\frac{4m_b^2}{c_\beta^2} - M_Z^2 \right) \log \frac{m_{\tilde{b}_2}^2 m_{\tilde{b}_1}^2}{Q^4} \right.$$

$$\begin{aligned}
& + \frac{M_Z^2 s_\beta}{4} \frac{(2m_b^2 k_t \mu \mathcal{R}_{b2} - c_\beta^2 \mathcal{X}_b)}{c_\beta(m_{b_2}^2 - m_{b_1}^2)} \log \frac{m_{b_2}^2}{m_{b_1}^2} \\
& + \frac{1}{4} \left(\frac{4m_b^2}{c_\beta} - M_Z^2 c_\beta \right) \frac{(2m_b^2 \mu \mathcal{R}_{b1} + c_\beta^2 \mathcal{X}_b)}{c_\beta(m_{b_2}^2 - m_{b_1}^2)} \log \frac{m_{b_2}^2}{m_{b_1}^2} \\
& + \frac{1}{4} \left(\frac{2k_t m_b^2 \mu^2 c_{\varphi_{kt}}}{c_\beta^2} - \mathcal{Z}_b(M_W, M_Z) s_{2\beta} \right) f(m_{b_1}^2, m_{b_2}^2) \\
& - \frac{(2m_b^2 \mu \mathcal{R}_{b1} + c_\beta^2 \mathcal{X}_b)(2k_t m_b^2 \mu \mathcal{R}_{b2} - c_\beta^2 \mathcal{X}_b)}{2c_\beta^2(m_{b_2}^2 - m_{b_1}^2)^2} g(m_{b_1}^2, m_{b_2}^2) \Big] \quad (21)
\end{aligned}$$

$$\begin{aligned}
\Delta_{13t} &= \frac{\beta_k}{2} \left[\frac{k_t m_t^2 \mu^2 t_\beta^{-1} s_{\varphi_{kt}}}{s_\beta} \left(-\frac{1}{2} f(m_{t_1}^2, m_{t_2}^2) - \frac{M_Z^2 \log \frac{m_{t_2}^2}{m_{t_1}^2}}{2(m_{t_2}^2 - m_{t_1}^2)} \right) \right. \\
& \left. + \frac{k_t m_t^2 \mu^2 s_{\varphi_{kt}} \left(m_t^2 \mu \mathcal{R}_{t1} + \frac{1}{2} s_{2\beta} \mathcal{X}_t \right)}{s_\beta^3(m_{t_2}^2 - m_{t_1}^2)^2} g(m_{t_1}^2, m_{t_2}^2) \right] \quad (22)
\end{aligned}$$

$$\begin{aligned}
\Delta_{13b} &= \frac{\beta_k}{2} \left[\frac{k_t m_b^2 \mu^2 s_{\varphi_{kt}}}{c_\beta} \left(-\frac{1}{2} f(m_{b_1}^2, m_{b_2}^2) - \left(\frac{2m_b^2}{c_\beta^2} - \frac{M_Z^2}{2} \right) \frac{\log \frac{m_{b_2}^2}{m_{b_1}^2}}{(m_{b_2}^2 - m_{b_1}^2)} \right) \right. \\
& \left. + \frac{k_t m_b^2 \mu^2 s_{\varphi_{kt}} \left(k_t m_b^2 \mu \mathcal{R}_{b2} - c_\beta^2 \mathcal{X}_b \right)}{c_\beta^3(m_{b_2}^2 - m_{b_1}^2)^2} g(m_{b_1}^2, m_{b_2}^2) \right] \quad (23)
\end{aligned}$$

$$\begin{aligned}
\Delta_{23t} &= \frac{\beta_k}{2} \left[\frac{k_t m_t^2 \mu^2 s_{\varphi_{kt}}}{s_\beta} \left(-\frac{1}{2} f(m_{t_1}^2, m_{t_2}^2) - \left(\frac{2m_t^2}{s_\beta^2} - \frac{M_Z^2}{2} \right) \frac{\log \frac{m_{t_2}^2}{m_{t_1}^2}}{(m_{t_2}^2 - m_{t_1}^2)} \right) \right. \\
& \left. + \frac{k_t m_t^2 \mu^2 s_{\varphi_{kt}} \left(2k_t m_t^2 \mu \mathcal{R}_{t2} - s_\beta^2 \mathcal{X}_t \right)}{s_\beta^3(m_{t_2}^2 - m_{t_1}^2)^2} g(m_{t_1}^2, m_{t_2}^2) \right] \quad (24)
\end{aligned}$$

$$\begin{aligned}
\Delta_{23b} &= \frac{\beta_k}{2} \left[\frac{k_t m_b^2 \mu^2 t_\beta s_{\varphi_{kt}}}{c_\beta} \left(-\frac{1}{2} f(m_{b_1}^2, m_{b_2}^2) - \frac{M_Z^2 \log \frac{m_{b_2}^2}{m_{b_1}^2}}{2(m_{b_2}^2 - m_{b_1}^2)} \right) \right. \\
& \left. + \frac{k_t m_b^2 \mu^2 s_{\varphi_{kt}} \left(m_b^2 \mu \mathcal{R}_{b1} + c_\beta^2 \mathcal{X}_b \right)}{c_\beta^3(m_{b_2}^2 - m_{b_1}^2)^2} g(m_{b_1}^2, m_{b_2}^2) \right] \quad (25)
\end{aligned}$$

where $\beta_k = \frac{3}{8\pi^2 g^2}$ and Q is the renormalization scale in the $\overline{\text{MS}}$ scheme. In the above expressions,

$$\begin{aligned}
\mathcal{R}_{t1} &= \mu \left(|k_t| c_{\varphi_{kt}} + t_\beta^{-1} \right) & \mathcal{R}_{t2} &= \mu \left(|k_t| + t_\beta^{-1} c_{\varphi_{kt}} \right), \\
\mathcal{R}_{b1} &= \mu \left(|k_t| c_{\varphi_{kt}} + t_\beta \right) & \mathcal{R}_{b2} &= \mu \left(|k_t| + t_\beta c_{\varphi_{kt}} \right). \quad (26)
\end{aligned}$$

and,

$$\mathcal{X}_t = \mathcal{Z}_t(M_W, M_Z)c_{2\beta}, \quad \mathcal{X}_b = -\mathcal{Z}_b(M_W, M_Z)c_{2\beta}. \quad (27)$$

where

$$\begin{aligned} \mathcal{Z}_t(M_W, M_Z) &= \left(\frac{4}{3}M_W^2 - \frac{5}{6}M_Z^2\right)^2, \\ \mathcal{Z}_b(M_W, M_Z) &= \left(\frac{2}{3}M_W^2 - \frac{1}{6}M_Z^2\right)^2, \end{aligned} \quad (28)$$

and the functions $f(m_{\tilde{t}_1(\tilde{b}_1)}^2, m_{\tilde{t}_2(\tilde{b}_2)}^2)$ and $g(m_{\tilde{t}_1(\tilde{b}_1)}^2, m_{\tilde{t}_2(\tilde{b}_2)}^2)$ are given by:

$$\begin{aligned} f(m_{\tilde{t}_1(\tilde{b}_1)}^2, m_{\tilde{t}_2(\tilde{b}_2)}^2) &= -2 + \log \frac{m_{\tilde{t}_1(\tilde{b}_1)}^2 m_{\tilde{t}_2(\tilde{b}_2)}^2}{Q^4} + \\ &\quad \frac{m_{\tilde{t}_2(\tilde{b}_2)}^2 + m_{\tilde{t}_1(\tilde{b}_1)}^2}{m_{\tilde{t}_2(\tilde{b}_2)}^2 - m_{\tilde{t}_1(\tilde{b}_1)}^2} \log \frac{m_{\tilde{t}_2(\tilde{b}_2)}^2}{m_{\tilde{t}_1(\tilde{b}_1)}^2} \end{aligned} \quad (29)$$

$$g(m_{\tilde{t}_1(\tilde{b}_1)}^2, m_{\tilde{t}_2(\tilde{b}_2)}^2) = -2 + \frac{m_{\tilde{t}_2(\tilde{b}_2)}^2 + m_{\tilde{t}_1(\tilde{b}_1)}^2}{m_{\tilde{t}_2(\tilde{b}_2)}^2 - m_{\tilde{t}_1(\tilde{b}_1)}^2} \log \frac{m_{\tilde{t}_2(\tilde{b}_2)}^2}{m_{\tilde{t}_1(\tilde{b}_1)}^2} \quad (30)$$

We diagonalize the Higgs mass-squared matrix (12) by the similarity transformation

$$\mathcal{R}M^2\mathcal{R}^T = \text{diag}(m_{h_1}^2, m_{h_2}^2, m_{h_3}^2), \quad (31)$$

where $\mathcal{R}\mathcal{R}^T = 1$, and we define h_3 to be the lightest of all three.

One of the most important quantities in our analyses is the percentage CP composition of a given mass-eigenstate Higgs boson. The percentage CP compositions of the Higgs bosons in terms of the basis elements are defined by

$$\rho_i = 100 \times |\mathcal{R}_{1i}|^2; \quad i = 1, 2, 3. \quad (32)$$

where ρ_1 , ρ_2 and ρ_3 correspond respectively the ϕ_1 , ϕ_2 , $\sin\beta\varphi_1 + \cos\beta\varphi_2$ components of the Higgs boson under concern. In the following, one of the main concerns will be the CP-odd composition ρ_3 , of the lightest Higgs boson as it can offer new opportunities at colliders for observing the Higgs boson[29, 40, 41, 42]. We will discuss the dependence of ρ_3 on different renormalization scales, as well as the interdependence of Q - μ , using the the previous theoretical [39], as well as the experimental results [38].

3 Numerical Analysis

In this section, we mainly address the phenomenological consequences of explicit radiative CP violation effects in the lightest Higgs boson, whose CP-odd composition as well as its mass are of prime importance in direct Higgs boson searches at high-energy colliders. As a result of the standard model Higgs boson searches at LEP, the lower bound on the lightest Higgs mass is 115 GeV (and correspondingly $\tan\beta \gtrsim 3.5$) [38]. On the other hand, theoretically the lightest Higgs boson mass can not exceed 130 GeV for large $\tan\beta$ [16]. Therefore, from the searches at LEP2, the lower limit on mass of the SM Higgs boson excludes the substantial part of the MSSM parameter space particularly (for $m_t = 175$ GeV), at small $\tan\beta$ ($\tan\beta \lesssim 3.5$) [38].

Being a reflecting property of the underlying model, all the soft masses are expressed in terms of the μ parameter, and since the μ parameter is already stabilized to the weak scale as a consequence of the naturalness, all dimensionless quantities are expected to be $\mathcal{O}(1)$. Therefore, we take all the dimensionless quantities in the $\mathcal{O}(1)$. In our numerical analysis, we study two specific values $\tan\beta$, namely $\tan\beta = 4$ and $\tan\beta = 30$, to analyze the CP violation effects on the lightest Higgs boson in the low and high $\tan\beta$ regimes.

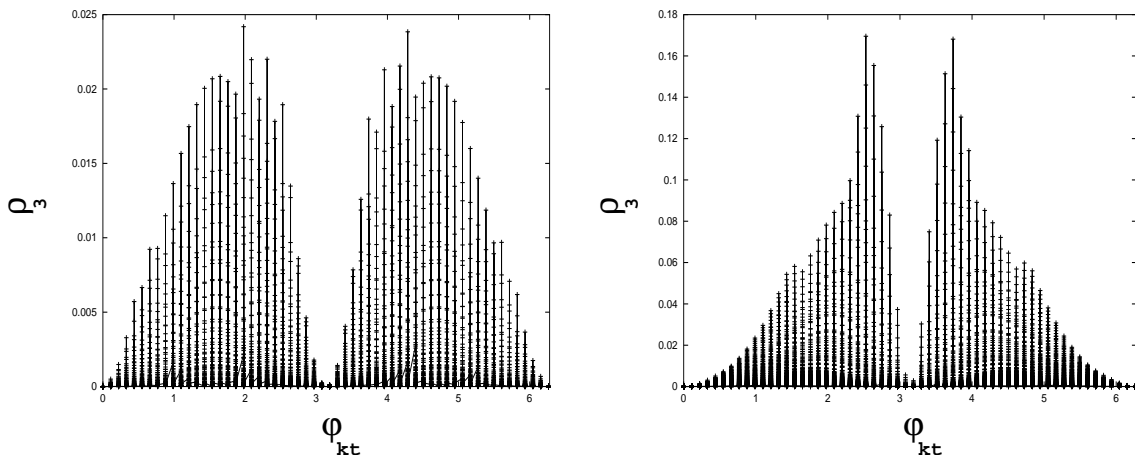


Figure 1: The CP-odd composition (ρ_3) of the lightest Higgs boson as a function of φ_{kt} , for $\tan\beta = 4$ (left panel), and $\tan\beta = 30$ (right panel), where Q varies from 175 GeV to 1200 GeV.

Shown in Fig. 1, is the φ_{kt} dependence of ρ_3 , designating the percentage CP-odd compositions of the lightest Higgs boson (h_3), for $\tan\beta = 4$ (left panel), and $\tan\beta = 30$ (right panel). In both panels Q changes from 175 GeV to 1200 GeV, and $|\mu|$ from 100 GeV to 1000 GeV in the full φ_{kt} range. Therefore, the variation of ρ_3 is represented by many points in the parameter space which correspond to different values of Q , and different values of μ . As is seen from both panels of Fig. 1, the maximal value of ρ_3 occurs at %0.025 for $\tan\beta = 4$, and at %0.17 for

$\tan\beta = 30$. Moreover, a comparative look at both windows shows that, although ρ_3 increases relatively with the increasing $\tan\beta$, it never exceeds %0.17 in the full φ_{kt} range, for all values of Q changing from 175 GeV to 1200 GeV. Compared to its CP-even compositions, which form the remaining percentage, this CP-odd component is extremely small to cause observable effects. It may, however, be still important when the radiative corrections to gauge and Higgs boson vertices are included [28].

The analysis of Fig. 1, gives a general idea of the variation of ρ_3 in the full φ_{kt} range. However, since the parameter space is quite large, for a better understanding of the properties of the model under concern, we focus on the different portions of parameter space corresponding to the different values of Q in Fig. 2. Therefore, in the left panel of Fig. 2, we choose three specific values of Q corresponding to 325 GeV ("+"), 600 GeV ("×"), 1000 GeV ("."), for $\tan\beta = 4$, and analyze the variation of ρ_3 in the full φ_{kt} range, for all values of μ changing from 100 GeV to 1000 GeV. On the other hand, we carry out the same analysis for $\tan\beta = 30$ in the right panel of Fig. 2. However, for convenience, starting from a lower value of Q , we let 190 GeV ("◇"), 325 GeV ("+"), 1000 GeV (".") values of Q for this case.

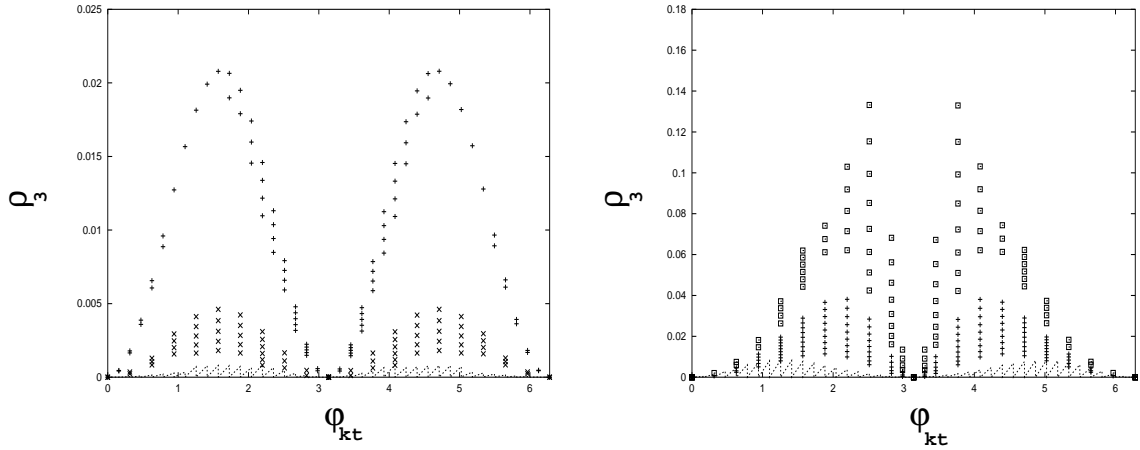


Figure 2: The CP-odd composition (ρ_3) of the lightest Higgs boson as a function of φ_{kt} , for $Q = 325$ GeV ("+"), 600 GeV ("×"), 1000 GeV ("."), for $\tan\beta = 4$ (left panel), and $Q = 190$ GeV ("◇"), 325 GeV ("+"), 1000 GeV ("."), for $\tan\beta = 30$ (right panel).

In Fig. 2, those portions of the parameter space which belong to different values of Q are presented by curves ("+", "×", ".", "◇"), and those curves correspond to different values of μ . A comparative look at $Q = 325$ GeV ("+"), and $Q = 600$ GeV ("×") scales, in the low $\tan\beta$ regime (left panel), shows that when $Q = 325$ GeV ("+"), and $\tan\beta = 4$ (left panel), there are very few curves, since the lower bound of μ (corresponding to $Q = 325$ GeV) starts from a rather higher value of μ ($\mu = 800$ GeV), and, it is not possible to find any allowed region below this

value ($\mu \lesssim 800\text{GeV}$), since the parameter space is constrained by the existing LEP bound on the lightest Higgs boson mass [38]. Moreover, even at this value of μ , one can not find solutions in the full φ_{kt} range, as will be shown in Fig. 3. Therefore, the allowed range of the parameter space is quite restricted for this case. At $Q = 600\text{GeV}$ and $\tan\beta = 4$ (left panel), ρ_3 decreases relatively as compared to the former case. However, as the allowed range of μ gradually gets widened, the number of curves increase (for instance, the lower bound of μ is 750GeV for this scale). On the other hand, ρ_3 is quite small at $Q = 1000\text{GeV}$, and $\tan\beta = 4$ (left panel), as compared to the other two scales ($Q = 325\text{GeV}$, $Q = 600\text{GeV}$). However, there is a gradual enlargement in the allowed range of μ (The allowed range of μ for all values of Q will be discussed in detail, in analyzing the $Q - \mu$ interdependence). The variation of $\rho_3 - \varphi_{kt}$ is similar in the high $\tan\beta$ regime (right panel of Fig. 2). Considering the portion of the parameter space which corresponds to $Q = 190\text{GeV}$ ("◇"), one notes that the parameter space is quite widened, even as compared to a larger scale, $Q = 325\text{GeV}$ ("+"), in the low $\tan\beta$ regime. On the other hand, a comparison between the left and right panels, at $Q = 325\text{GeV}$, also shows that, the number of curves, namely the allowed range of μ increases gradually, as well as ρ_3 , in the high $\tan\beta$ regime (right panel).

From the analysis of Figs. 1, 2, we can conclude that the allowed range of μ , as well as ρ_3 gradually increases with the increasing $\tan\beta$. However, as the $\rho_3 - \mu$ dependence is taken into consideration, it is seen that some differences arise in connection with the different values of Q . Therefore, to understand the properties of different values of Q , and in particular their influences on ρ_3 , as well as on μ , we carry out the same analysis from a slightly different perspective in Figs. 3, 4, 5 focusing on the behaviour of the small, moderate and large values of Q , under different values of μ , in both regimes

Shown in Fig. 3, is the variation of the CP-odd composition (ρ_3) of the lightest Higgs boson as a function of φ_{kt} , for $\tan\beta = 4$ (left panel), and $\tan\beta = 30$ (right panel), when $\mu = 800\text{ GeV}$. The three different curves present three different values of Q corresponding to 325 GeV (top curve), 600 GeV (middle curve), 1000 GeV (bottom curve), respectively. The same analysis has been carried out for $\mu = 900\text{ GeV}$ in Fig. 4, and, for $\mu = 1000\text{ GeV}$ in Fig. 5. As is seen from the left panel of Fig. 3, at $Q = 325\text{ GeV}$, and $\mu = 800\text{ GeV}$ (the lower bound of μ for this scale), there are solutions only in a small portion of parameter space in the full φ_{kt} range, which corresponds to $[4\pi/5, 6\pi/5]$ interval, since one can not find any allowed region satisfying the experimental constraint [38] beyond this interval. At $Q = 325\text{ GeV}$, and $\mu = 900\text{ GeV}$ (left panel of Fig. 4), the allowed range of φ_{kt} slightly widens. One notes that, for $Q = 325\text{ GeV}$, the experimental constraint is satisfied in the full φ_{kt} range, only at $\mu = 1000\text{ GeV}$ (left panel of Fig. 5). On the other hand, as the renormalization scale increases, for instance, at $Q = 600\text{ GeV}$,

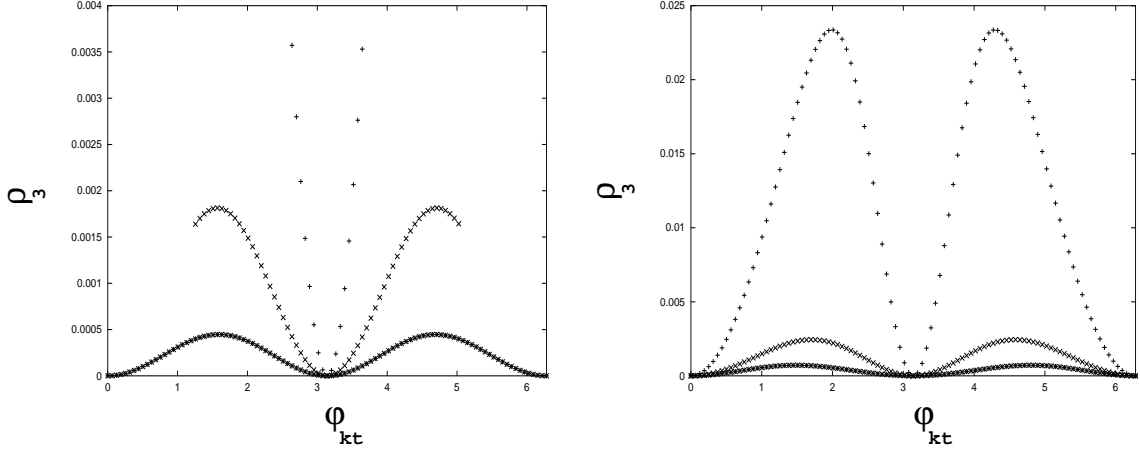


Figure 3: The CP-odd composition (ρ_3) of the lightest Higgs boson as a function of φ_{kt} , for $\tan \beta = 4$ (left panel), and $\tan \beta = 30$ (right panel), and $\mu = 800$ GeV, where the top, middle and bottom curves correspond to $Q = 325$ GeV ("+"), 600 GeV ("x"), 1000 GeV ("*") respectively.

the allowed range of φ_{kt} gradually gets widened, and at $Q = 1000$ GeV, there are solutions in the full φ_{kt} range. Similar observations can be made for the $\tan \beta = 30$ case. However, as is seen from the right panels of Figs. 3, 4, 5 that the experimental constraint is satisfied for all values of φ_{kt} in this regime.

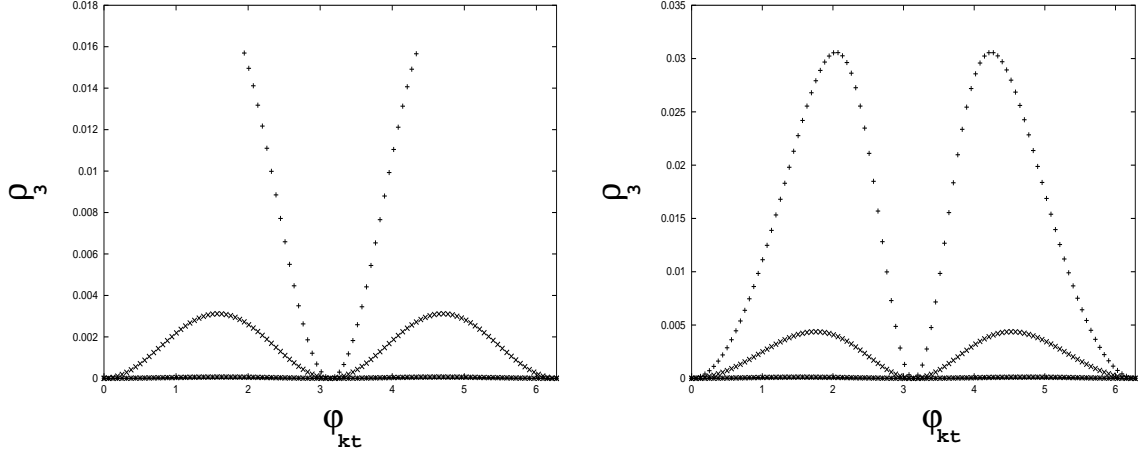


Figure 4: The same as Fig. 3, but for $\mu = 900$ GeV

Moreover, as is shown in the left panel of Fig. 4, for $Q = 325$ GeV, the maximal value of ρ_3 occurs at ~ 0.004 for $\mu = 800$ GeV. Then, increasing slightly, and it reaches to ~ 0.016 at $\mu = 900$ GeV (the left panel of Fig. 5). Finally, the maximum value of ρ_3 occurs at ~ 0.022 at $\mu = 1000$ GeV (left panel of Fig. 6). On the other hand, ρ_3 slightly decreases for $Q = 600$ GeV, as compared to the former case ($Q = 325$ GeV), and like the former case, its ρ_3 - μ dependence is

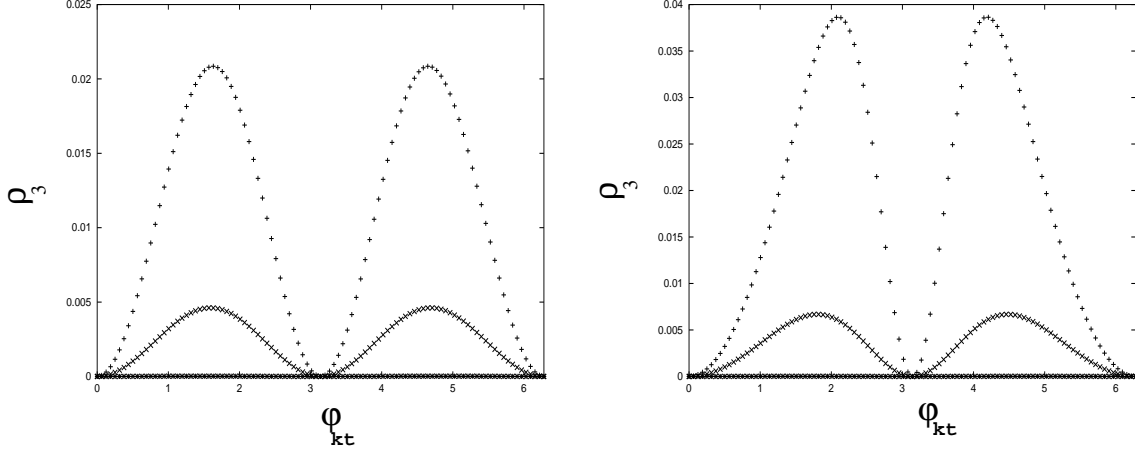


Figure 5: The same as Fig. 3, but for $\mu = 1000$ GeV

of the same kind (the larger μ , the larger ρ_3). In passing to $Q = 1000$ GeV, one notes from the left panel of Fig. 3 that, ρ_3 decreases relatively as compared to $Q = 325$ GeV, and $Q = 600$ GeV cases, and it occurs maximally at ~ 0.0005 at $\mu = 800$ GeV. However, unlike the $Q = 325$ GeV and $Q = 600$ GeV cases, ρ_3 (corresponding to $Q = 1000$ GeV) is smaller at $\mu = 900$ GeV than that of $\mu = 800$ GeV, and in fact, it reaches to its minimal value at $\mu = 1000$ GeV (which will be seen in detail in analyzing the $\rho_3 - \mu$ interdependence of $Q = 1000$ GeV).

Therefore, the comparative analysis of Figs. 3, 4 and 5 shows that, there are differences in the ρ_3 - μ dependence of Q in both low and high $\tan \beta$ regimes, in the sense that, although ρ_3 increases with increasing μ for $Q = 325$ GeV, and, $Q = 600$ GeV, its dependence on μ changes in passing to the higher renormalization scales (for instance at $Q = 1000$ GeV, ρ_3 decreases with increasing μ). Therefore, one can deduce from the above analysis that, there should be critical values of Q in both low and high $\tan \beta$ regimes, beyond which the ρ_3 - μ dependence changes. To determine these portions of the parameter space, it is necessary to discuss the variation of ρ_3 with Q , which will be carried out in the following.

Before analyzing the dependence of Q on ρ_3 in the full φ_{kt} range from a general point of view, we focus on a smaller portion of a parameter space, for clearance. Therefore, in Fig. 6, we choose a particular value of φ_{kt} , namely, we set $\varphi_{kt} = 3\pi/2$. Moreover, as Q changing from 175 GeV to 1200 GeV, we let 975 GeV ("*"), 875 GeV ("x"), 775 GeV ("+"), 675 GeV ("diamond") values of μ , for $\tan \beta = 4$ (left panel), and $\tan \beta = 30$ (right panel). One notes that, there is no allowed region in the parameter space corresponding to $\mu = 675$ GeV for $\tan \beta = 4$ (left panel). In fact, it is not possible to find any region in the parameter space below $\mu \lesssim 700$ for $\tan \beta = 4$ (this bound is $\mu \lesssim 500$ for $\tan \beta = 30$), due to the experimental constraint on the lower bound of the lightest Higgs mass [38]. Thus, in choosing the different values of μ , we try to form the most

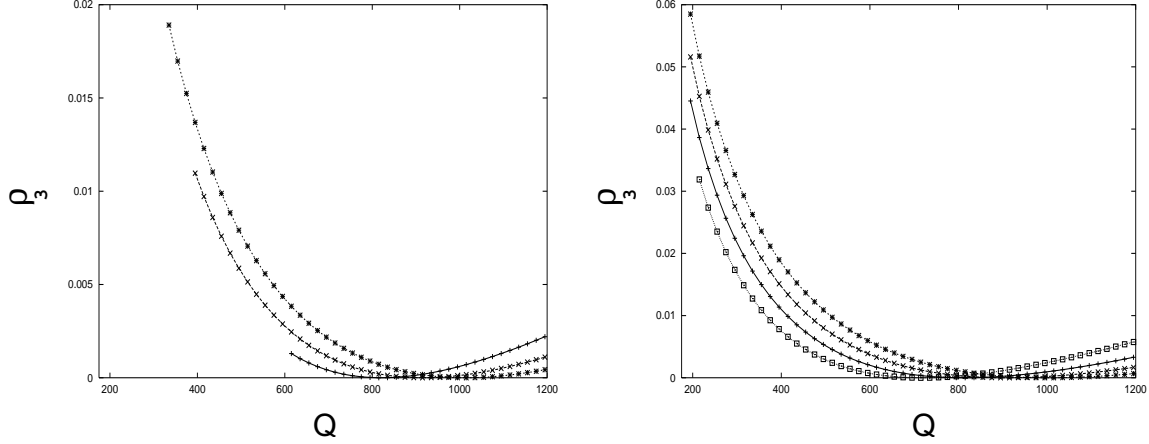


Figure 6: The CP-odd composition (ρ_3) of the lightest Higgs boson as a function of the renormalization scale Q , at $\varphi_{kt} = 3\pi/2$, for $\tan\beta = 4$ (left panel), and $\tan\beta = 30$ (right panel), with different values of μ corresponding to $\mu = 975\text{GeV}$ ("*"), 875GeV ("x"), 775GeV ("+"), 675GeV ("◇")

suitable combination. In Fig. 6, for the ease of following we cut the vertical axes $\rho_3 = 0.02\%$ for $\tan\beta = 4$ (left panel), and $\rho_3 = 0.06\%$ for $\tan\beta = 30$ (right panel). However, as will be seen in Fig. 7, it actually extends to 0.025% for $\tan\beta = 4$, and 0.18% for $\tan\beta = 30$ in the full φ_{kt} interval. Although the analysis has been carried out for a particular value of φ_{kt} ($\varphi_{kt} = 3\pi/2$), one notes that there are two portions in the parameter space. In the first portion, ρ_3 decreases with decreasing μ , then after a certain value of Q , in the second portion, ρ_3 starts to increase slightly with decreasing μ . For instance, as is seen from the left panel of Fig. 6, in the first portion of the parameter space ($Q \lesssim 925\text{GeV}$), the maximal value of ρ_3 occurs at $\mu = 975\text{GeV}$ ("*"), and it decreases slightly with the decrease in μ . On the other hand, in the second portion of the parameter space ($Q \gtrsim 925\text{GeV}$), the maximal value of ρ_3 is smaller than that of the first region. However, ρ_3 is maximal at $\mu = 775\text{GeV}$ ("+"), and, unlike the first portion of the parameter space, ρ_3 lessens as μ increases. For instance, ρ_3 is minimal at $\mu = 975\text{GeV}$ ("*"), in the second portion. Similar observations can be made also for the high $\tan\beta$ regime. Clearly, with the analysis of Fig. 5, we focus on a particular value of φ_{kt} , and try to understand the ρ_3 - μ dependence of Q , considering different values of μ . In the following, we will carry out the same analysis from a more general point of view, which will provide us to determine the critical values of Q more precisely, and to understand the properties of the model under concern in more detail.

In Fig. 7, we show the variation of ρ_3 with Q for $\tan\beta = 4$ (left panel), and $\tan\beta = 30$ (right panel) in the full φ_{kt} range. In each panel, Q ranges from 175 GeV to 1200 GeV , μ from 100 GeV to 1000 GeV . Here, the vertical lines represent different values of φ_{kt} , as well

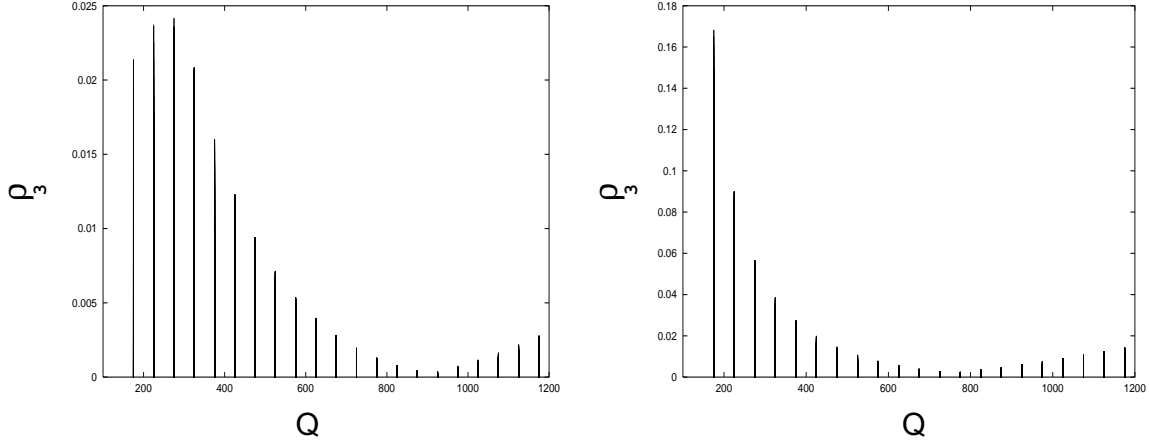


Figure 7: The CP-odd composition (ρ_3) of the lightest Higgs boson as a function of the renormalization scale Q , for $\tan \beta = 4$ (left panel), and $\tan \beta = 30$ (right panel).

as different values of μ , as was indicated in Fig. 6. As is seen from the left panel of Fig. 7, the maximum value of ρ_3 ($\sim 0.025\%$) occurs at $Q = 275$ GeV. For larger values of Q , ρ_3 decreases gradually until $Q = 925$ GeV, as the supersymmetric spectrum decouples. One notes that, beyond this point ρ_3 starts to increase slightly. For smaller values of Q , however, the parameter space is constrained by the existing LEP bound on the lightest Higgs mass [38]. That is, ρ_3 gets smaller until $Q = 175$ GeV, and it is not possible to find any region in the parameter space below this value ($Q \lesssim 175$ GeV), for $\tan \beta = 4$, since this region is completely disallowed by the experimental bound [38]. On the other hand, as is shown in the right panel of Fig. 7, the maximum value of ρ_3 ($\sim 0.17\%$) occurs at $Q = 175$ GeV for $\tan \beta = 30$. Similar to the low $\tan \beta$ regime, ρ_3 decreases with increasing Q until $Q = 775$ GeV, and beyond this point there is a small increase in ρ_3 in the admitted range of Q .

Following the analysis of Figs. 3-7, we would like to emphasize that in the first portion of the parameter space ($175 \lesssim Q \lesssim 925$ for $\tan \beta = 4$, and $175 \lesssim Q \lesssim 775$ for $\tan \beta = 30$), as μ increases with increasing ρ_3 (Figs. 3-6), ρ_3 decreases with increasing Q (Figs. 6-7). On the other hand, in the second portion of the parameter space ($925 \lesssim Q \lesssim 1200$ for $\tan \beta = 4$, and $775 \lesssim Q \lesssim 1200$ for $\tan \beta = 30$), ρ_3 gradually increases with increasing Q (Figs. 6-7), and since this increase in ρ_3 is compensated by the decrease in μ , unlike the first region, μ decreases with increasing ρ_3 (see Fig. 3-6). Therefore, the interdependence of $\mu - \rho_3$ changes in this region (see Fig. 6). However, the maximal values of ρ_3 never exceeds $\sim 0.005\%$ for $\tan \beta = 4$, and $\sim 0.02\%$ for $\tan \beta = 30$, in the second portion of the parameter space. Obviously if the lightest Higgs boson were carrying large enough CP-odd composition, this would bring about new opportunities for observing the lightest Higgs in the near future. However, one notes that as the CP violation

effects are induced only radiatively in the MSSM and in the model at hand, it is clear that any would-be observation of a large CP violating composition of the lightest Higgs boson at LHC, or NLC, or TESLA excludes the MSSM in general, and the model under concern in particular.

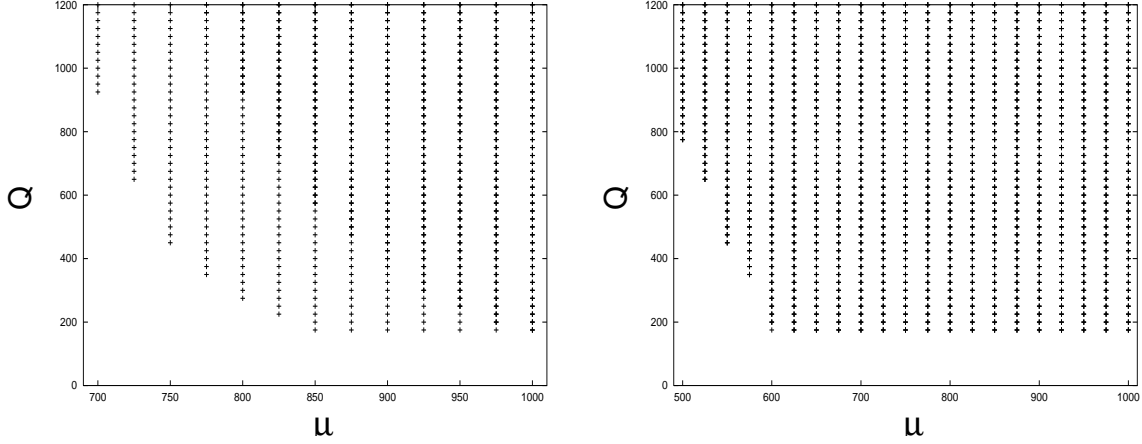


Figure 8: The dependence of the renormalization scale Q on $|\mu|$ for $\tan \beta = 4$ (left panel), and $\tan \beta = 30$ (right panel).

In Fig. 8, we show the interdependence of Q on $|\mu|$ for $\tan \beta = 4$ (left panel), and $\tan \beta = 30$ (right panel). In each panel Q varies from 175 GeV to 1200 GeV, and μ from 100 GeV to 1000 GeV. As is seen from the left panel, in the first portion of the parameter space, starting from $Q = 175$ GeV, the range of Q gets widened up to $Q = 925$ GeV, whereas the lower allowed bound of μ changes from 850 GeV to 700 GeV in this interval. For instance, at $Q = 325$ GeV and $\tan \beta = 4$, the lower bound of μ starts from 800 GeV (see Fig. 3), and, at 600 GeV, it decreases to 750 GeV in the same regime, as will be shown in Fig. 9. On the other hand, in the second portion of the parameter space ($925 \lesssim Q \lesssim 1200$), the allowed range of μ remains constant. That is, all values of μ changing from 700 GeV to 1000 GeV are allowed for $Q \gtrsim 925$ (for instance, the lower bound of μ , corresponding to $Q = 1000$ GeV starts from 700 GeV, as will be indicated in Fig. 10). Q - μ interdependence is similar at large $\tan \beta$ (right panel). However, in this regime, as the range of Q gradually widens in the $175 \lesssim Q \lesssim 775$ GeV interval, the lower bound on μ changes from 600 GeV to 500 GeV. Above this interval ($Q \gtrsim 775$), all values of μ , from 500 GeV to 1000 GeV are allowed. For instance, the lower bound of μ , corresponding to 600 GeV starts from $\mu = 550$ GeV at $\tan \beta = 30$, whereas it is $\mu = 500$ GeV, for $Q = 1000$ GeV in the same regime, beyond which all values of μ are allowed (see Figs. 9-10).

We would like to remind that in the present analysis, the allowed range of the parameter space is obtained by imposing the recent LEP constraint on the lightest Higgs mass (m_{h_3}) which requires $m_{h_3} \gtrsim 115$ GeV [38]. As is seen from both panels of Fig. 8, the lower bound on μ

starts from 700GeV for $\tan\beta = 4$ (left panel), whereas this bound decreases to 500GeV for $\tan\beta = 30$ (right panel), and it is not possible to find any region in the parameter space below these values ($\mu \lesssim 700\text{GeV}$ for $\tan\beta = 4$, and $\mu \lesssim 500\text{GeV}$ for $\tan\beta = 30$), since these regions of the parameter space are completely disallowed by the existing LEP bound on the lightest Higgs mass [38]. Moreover, it is worthwhile of mentioning that the present analysis includes the dominant top-stop contributions, as well as the bottom-sbottom effects, whereas the two-loop corrections have not been taken into account. In this case, the approximation used here for the calculation still contains a theoretical error of several GeV [43]. Therefore, the allowed range might change mildly, in case of a higher precisional calculation.

With the former analysis, we have studied the properties of the model under concern, as the Q -dependence is taken into the consideration. At this point, we come back to the question mentioned in the purpose of this work (whether one can find an appropriate limit of reasonable agreement with the scale independent results [39]). Therefore, in Fig. 9, we focus on two particular values of Q , namely $Q = 600$ GeV, and $Q = 1000$ GeV, and investigate their $\rho_3 - \mu$ dependence in both high and low $\tan\beta$ regimes.

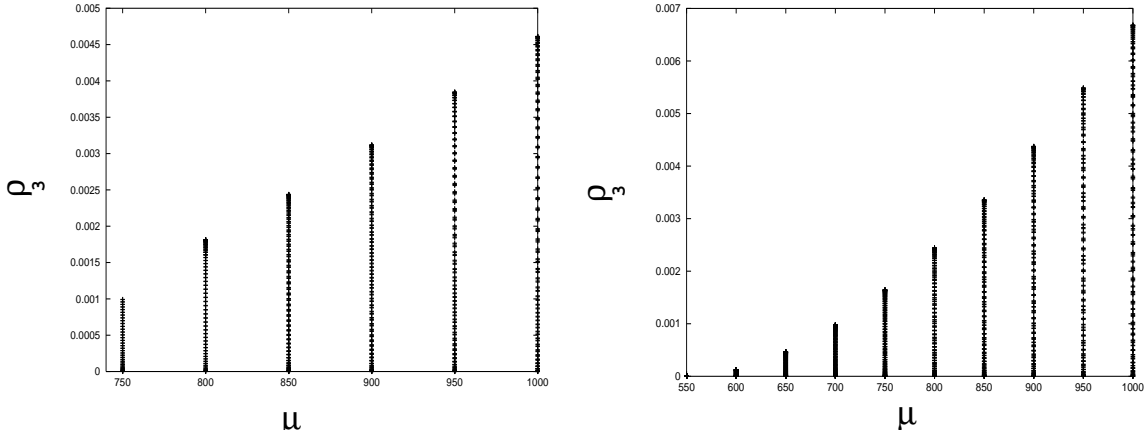


Figure 9: The CP-odd composition (ρ_3) of the lightest Higgs boson as a function of $|\mu|$ for $Q = 600$ GeV, when $\tan\beta = 4$ (left panel), and $\tan\beta = 30$ (right panel)

Depicted in Fig. 9 is the $|\mu|$ dependence of ρ_3 for $\tan\beta = 4$ (left panel), and $\tan\beta = 30$ (right panel) at $Q = 600$ GeV. In Fig. 10, the same dependence is shown for a larger scale, namely for $Q = 1000$ GeV. In both panels, the vertical lines correspond to different phases in the full φ_{kt} range (see Figs. 3, 4, 5). A comparative glance at both panels shows that, in both high and low $\tan\beta$ regimes, the $\rho_3 - \mu$ dependence at $Q = 600$ GeV scale differs from that of $Q = 1000$ GeV. In fact, the $\rho_3 - \varphi_{kt}$ dependence corresponding to these scales has been analyzed in Figs. 3, 4, 5, and the critical values of Q (beyond which $\rho_3 - \mu$ behaviour changes) has been determined in

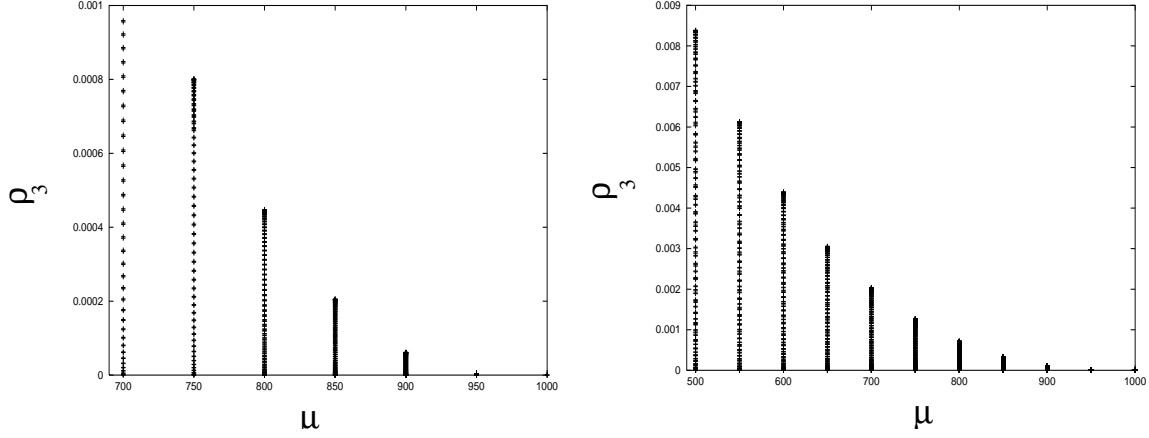


Figure 10: The same as Fig. 9 , but for $Q = 1000$ GeV.

Figs. 6, 7. Therefore, such kind of behaviour is expected, remembering that in the first portion of the parameter space ($175 \lesssim Q \lesssim 925$ for $\tan \beta = 4$, and $175 \lesssim Q \lesssim 775$ for $\tan \beta = 30$), μ increases with increasing ρ_3 (Fig. 7), whereas it decreases with increasing ρ_3 in the second portion of the total Q range ($925 \lesssim Q \lesssim 1200$ for $\tan \beta = 4$, and $775 \lesssim Q \lesssim 1200$ for $\tan \beta = 30$). As is seen from the left panel of Fig. 9, at $Q = 600$ GeV, and $\tan \beta = 4$, the maximum value of ρ_3 ($\sim 0.005\%$) occurs at $\mu = 1000$ GeV, and for smaller values of μ , ρ_3 decreases gradually. In passing to $\tan \beta = 30$ case (right panel), one observes that as ρ_3 increases slightly, the allowed range of μ widens (the lower bound on μ decreases to $\mu = 550$ GeV). On the other hand, as is seen from the left panel of Fig. 10, at $Q = 1000$ GeV, and $\tan \beta = 4$, the maximal value of ρ_3 ($\sim 0.001\%$) occurs at $\mu = 700$ GeV, and unlike the $Q = 600$ GeV case, for larger values of μ , ρ_3 decreases gradually. The variation of ρ_3 with μ , for $\tan \beta = 30$ (right panel of Fig. 10) is similar to what we have observed in the $\tan \beta = 4$ regime (left panel of Fig. 10). However, there is a gradual increase in ρ_3 , as well as the allowed range of μ , for $\tan \beta = 30$.

We would like to note that the variation of ρ_3 with μ (Fig. 10), which corresponds to $Q = 1000$ GeV, is very similar to what we have found in [39]. This particular result shows that the scale dependence of the radiative corrections is sufficiently suppressed for the renormalization scale $Q = 1000$ GeV. On the other hand, consideration of various renormalization scales, all being around the weak scale, lead us to a wealth of CP violation opportunities. This is especially suggested by Fig. 9, where the percentage CP-odd composition of the lightest Higgs gradually increases with μ .

As mentioned above, among the values of Q changing from 175 GeV to 1200 GeV, of particular interest is the $Q = 1000$ GeV where the comparison between the results of this work and that of [39] is possible, and a reasonable agreement with [39] can be found. Shown in Fig. 11,

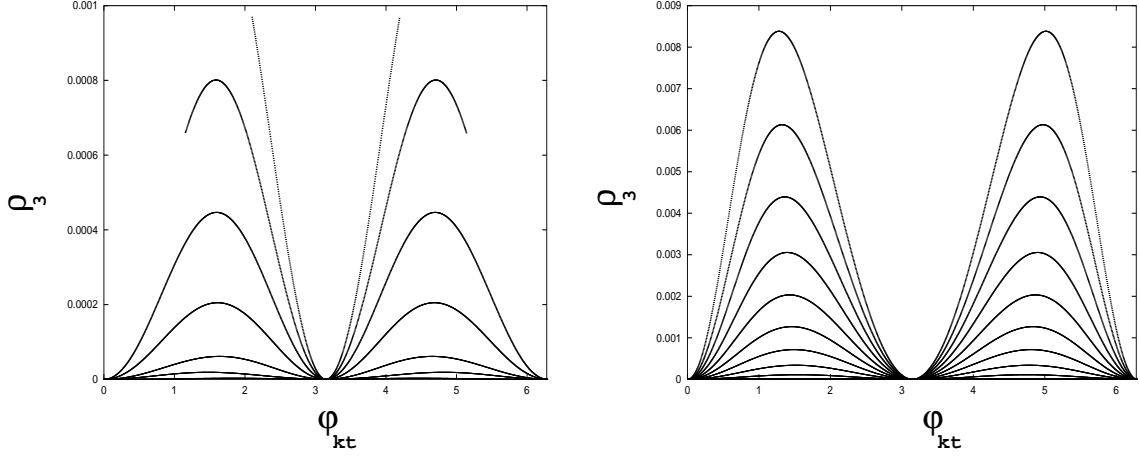


Figure 11: The dependence of the CP-odd composition (ρ_3) of the lightest Higgs boson on φ_{kt} , corresponding to $Q = 1000\text{GeV}$, for $\tan\beta = 4$ (left panel), and $\tan\beta = 30$ (right panel)

is the φ_{kt} dependence of the percentage CP-odd compositions of the lightest Higgs boson (ρ_3), corresponding to $Q = 1000\text{ GeV}$, for $\tan\beta = 4$ (left panel), and $\tan\beta = 30$ (right panel). As both panels of the figure suggests the maximal value of ρ_3 occurs at $\sim 0.001\%$ for $\tan\beta = 4$ (left panel), and increasing slightly it reaches to $\sim 0.009\%$ for $\tan\beta = 30$ (right panel), in the full φ_{kt} range. As has been shown in Figs. 3,4,5 each curve in the figure represents different values of μ . For instance, in the $\tan\beta = 4$ regime (left panel) the curve on the top corresponds to the lower bound of μ ($\mu = 700\text{GeV}$), for which ρ_3 reaches its maximal (see Fig. 10), and similarly from the top curve to the bottom with the increase in μ , ρ_3 decreases. Similar to observations made for the left panel, one can discuss the high $\tan\beta$ regime (right panel), where the top curve corresponds to the lower bound of μ ($\mu = 500\text{GeV}$), for $\tan\beta = 30$ (see Fig. 10). One notes that, the ρ_3 reaches maximally to $\sim 0.009\%$ in the full φ_{kt} range, for all values of $\tan\beta$ changing from 4 to 30.

As is explained in the Introduction, considering only the dominant top-stop quark loops, and being the results of Q -independent, the variation of ρ_3 with φ_{kt} is analyzed in [39], and it has been found that the maximal value of ρ_3 never exceeds 0.0013% for all values of $\tan\beta$ changing 4 to 30 in the full φ_{kt} range (the maximal values of $\rho_3 \sim 0.0003\%$ for $\tan\beta = 4$, and $\rho_3 \sim 0.0013\%$ for $\tan\beta = 30$ in [39]) The dependence of ρ_3 on φ_{kt} (see Fig. 10), which corresponds to $Q = 1000\text{ GeV}$, is very similar to that of [39]. However, one notes that maximal value of ρ_3 slightly increases in this work, as compared to the former analysis.

Among the particles contributing to the one-loop radiative corrections, the dominant ones come from the top quark and top squark loops, provided that $\tan\beta \lesssim 50$, (for which case the bottom Yukawa coupling is quite small to give significant contributions). The Yukawa interac-

tions due to scalar bottom quarks can be significant only for very large $\tan\beta$ values. Therefore, by the inclusion of the bottom-sbottom loops ρ_3 increases slightly as expected, however, it never exceeds 0.009%, for all values of $\tan\beta$ changing from 4 to 30.

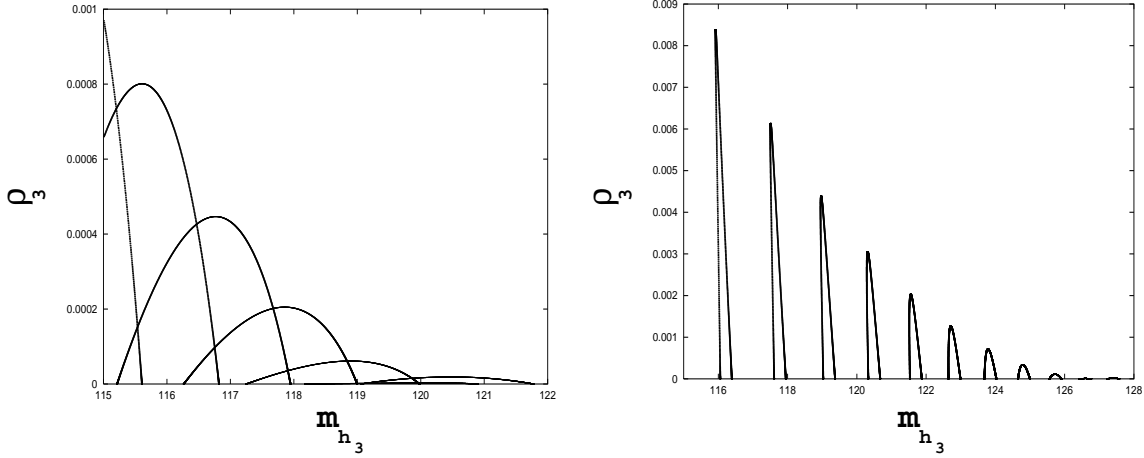


Figure 12: The dependence of the mass of the lightest Higgs boson (m_{h_3}) on φ_{kt} , corresponding to $Q = 1000\text{GeV}$, for $\tan\beta = 4$ (left panel), and $\tan\beta = 30$ (right panel)

Finally, depicted in Fig. 12, is the variation of ρ_3 with m_{h_3} , corresponding to $Q = 1000\text{ GeV}$, for $\tan\beta = 4$ (left panel), and for $\tan\beta = 30$ (right panel). The decreasing curves in each panel represent different values of φ_{kt} , and μ as well. The maximal value of ρ_3 occurs at $\sim 0.001\%$, and correspondingly at $\mu = 700\text{GeV}$ (see Figs. 10, 11). Then, it decreases rapidly with the increasing mass, and decreasing μ . For instance, it reaches to $\rho_3 \sim 0.0005\%$ at $\mu = 800\text{GeV}$ (see Figs. 3, 10, 11), for $\tan\beta = 4$ (left panel). Similar observations can be made for the right panel, in which case the maximal value of $\rho_3 \sim 0.009\%$ occurs at $\mu = 500\text{GeV}$ (see Fig. 11), and like the former case, it decreases relatively with the increasing mass again. For instance, $\rho_3 \sim 0.005\%$, at $\mu = 800\text{GeV}$ (see Figs. 3, 10, 11). Finally, it reaches far below $\rho_3 \sim 0.001\%$ for $m_{h_3} = 127\text{GeV}$.

As both panels of the figure shows that lighter the Higgs boson (h_3) larger its CP-odd composition. Therefore, as the ρ_3 - m_{h_3} dependence (which corresponds to $Q = 1000\text{ GeV}$) suggests, any possible increase in the lower experimental bound of the lightest Higgs mass will imply reduced CP-odd composition, being in a reasonable agreement with the results of [39].

Before concluding, we would like to note that we have concentrated on a particular scale $Q = 1000\text{ GeV}$, for which case the results are very similar to what we have found in the scale-independent case [39]. In fact, in both low and high $\tan\beta$ regimes, $Q = 1000\text{ GeV}$, is an approximately intersectional value of the second portion of the parameter space ($925 \lesssim Q \lesssim 1200$ for $\tan\beta = 4$, and $775 \lesssim Q \lesssim 1200$ for $\tan\beta = 30$), beyond which the $\rho_3 - \mu$ dependence

changes. Moreover, if we consider the remaining interval in the second portion of the parameter space $1000 \lesssim Q \lesssim 1200$, similar results can be obtained. Naturally, in the $1000 \lesssim Q \lesssim 1200$ interval, with the decrease in μ , ρ_3 increases gradually, which is a characteristic behaviour of the second portion of the parameter space (see Fig. 7). However ρ_3 never exceeds $\sim 0.02\%$ even at $Q = 1200$ GeV. Therefore, one can conclude that there is a strong influence of Q on the ρ_3 - μ interdependence in the first portion of the parameter space ($175 \lesssim Q \lesssim 925$ for $\tan\beta = 4$, and $175 \lesssim Q \lesssim 775$ for $\tan\beta = 30$). On the other hand, the scale dependence of the radiative corrections is sufficiently suppressed in the second portion of the parameter space, in particular, $1000 \lesssim Q \lesssim 1200$, interval, for both low and high $\tan\beta$ regimes.

4 Conclusion

In this work, we have mainly concentrated on the percentage CP odd-compositions of the lightest Higgs boson, with the inclusion of the bottom-sbottom contributions, for all values of Q ranging from top mass to TeV scale. We would like to briefly summarize the results:

1. A comparative glance at both low and high $\tan\beta$ regimes shows that as Q increases, the percentage CP-odd composition of the lightest Higgs (ρ_3) decreases until $Q = 925\text{GeV}$ for $\tan\beta = 4$, and $Q = 775\text{GeV}$ for $\tan\beta = 30$. Beyond these points, ρ_3 gradually starts to increase in the admitted range of Q . However, it never exceeds 0.17% for all values of Q changing from 175 GeV to 1200 GeV. As compared to its percentage CP-even compositions this value is so small to cause observable effects. Therefore, lightest Higgs remains essentially CP even.
2. The present analysis differs from that of [39], in the sense that the latter does not depend on Q explicitly since the D-term as well as the bottom-sbottom contributions are not taken into the consideration. However, in the appropriate limit, namely for $Q = 1000\text{GeV}$, a comparison between the results is possible, and a reasonable agreement with [39] can be found. Moreover, similar observations can be made for the second portion of the parameter space, particularly in the $1000 \lesssim Q \lesssim 1200$ interval, which is an allowed intersectional region in both low and high $\tan\beta$ regimes. Therefore, one can conclude that there is a strong influence of Q on the $\rho_3 - \mu$ interdependence in the first portion of the parameter space. On the other hand, the scale dependence of the radiative corrections is sufficiently suppressed for the second portion of the parameter space, particularly in the $1000 \lesssim Q \lesssim 1200$ interval. However, consideration of various renormalization scales, all being around the weak scale, lead us to a wealth of CP violation opportunities.

3. The underlying model provides a quite restricted parameter space due to the naturalness requirements, as well as a simultaneous solution both to the the strong CP and μ -problems.

M. B would like to thank the Scientific and Technical Research Council of Turkey (TÜBİTAK) for partial support under the project, No:TBAG2002(100T108).

References

- [1] H. E. Haber and R. Hempfling, Phys. Rev. Lett. **66** (1991) 1815.
- [2] Y. Okada, M. Yamaguchi and T. Yanagida, Prog. Theor. Phys. **85** (1991) 1.
- [3] J. R. Ellis, G. Ridolfi and F. Zwirner, Phys. Lett. B **257** (1991) 83.
- [4] J. R. Ellis, G. Ridolfi and F. Zwirner, Phys. Lett. B **262** (1991) 477.
- [5] R. Hempfling and A. H. Hoang, Phys. Lett. B **331** (1994) 99 [arXiv:hep-ph/9401219].
- [6] P. H. Chankowski, S. Pokorski and J. Rosiek, Nucl. Phys. B **423** (1994) 497.
- [7] Y. Okada, M. Yamaguchi and T. Yanagida, Phys. Lett. B **262** (1991) 54.
- [8] K. Sasaki, M. Carena and C. E. Wagner, Nucl. Phys. B **381** (1992) 66.
- [9] H. E. Haber and R. Hempfling, Phys. Rev. D **48** (1993) 4280 [arXiv:hep-ph/9307201].
- [10] J. A. Casas, J. R. Espinosa, M. Quiros and A. Riotto, Nucl. Phys. B **436** (1995) 3 [Erratum-ibid. B **439** (1995) 466] [arXiv:hep-ph/9407389].
- [11] M. Carena, M. Quiros and C. E. Wagner, Nucl. Phys. B **461** (1996) 407 [arXiv:hep-ph/9508343].
- [12] M. Carena, J. R. Espinosa, M. Quiros and C. E. Wagner, Phys. Lett. B **355** (1995) 209 [arXiv:hep-ph/9504316].
- [13] H. E. Haber, R. Hempfling and A. H. Hoang, Z. Phys. C **75** (1997) 539 [arXiv:hep-ph/9609331].
- [14] J. R. Espinosa and R. J. Zhang, JHEP **0003** (2000) 026 [arXiv:hep-ph/9912236].
- [15] M. Carena, H. E. Haber, S. Heinemeyer, W. Hollik, C. E. Wagner and G. Weiglein, Nucl. Phys. B **580** (2000) 29 [arXiv:hep-ph/0001002].

- [16] S. Heinemeyer, W. Hollik and G. Weiglein, Phys. Lett. B **440** (1998) 296 [arXiv:hep-ph/9807423].
- [17] A. Pilaftsis, Phys. Lett. B **435** (1998) 88 [arXiv:hep-ph/9805373].
- [18] A. Pilaftsis, Phys. Rev. D **58** (1998) 096010 [arXiv:hep-ph/9803297].
- [19] A. Pilaftsis and C. E. Wagner, Nucl. Phys. B **553** (1999) 3 [arXiv:hep-ph/9902371].
- [20] D. A. Demir, Phys. Rev. D **60** (1999) 055006 [arXiv:hep-ph/9901389].
- [21] S. W. Ham, S. K. Oh, E. J. Yoo and H. K. Lee, J. Phys. G **27** (2001) 1.
- [22] T. Ibrahim and P. Nath, Phys. Rev. D **63** (2001) 035009 [arXiv:hep-ph/0008237].
- [23] S. Y. Choi, M. Drees and J. S. Lee, Phys. Lett. B **481** (2000) 57 [arXiv:hep-ph/0002287].
- [24] M. Carena, J. R. Ellis, A. Pilaftsis and C. E. Wagner, Nucl. Phys. B **586** (2000) 92 [arXiv:hep-ph/0003180].
- [25] M. Dugan, B. Grinstein and L. J. Hall, Nucl. Phys. B **255** (1985) 413.
- [26] P. Nath, Phys. Rev. Lett. **66** (1991) 2565.
- [27] Y. Kizukuri and N. Oshimo, Phys. Rev. D **45** (1992) 1806.
- [28] D. A. Demir, Phys. Lett. B **465** (1999) 177 [arXiv:hep-ph/9809360].
- [29] D. A. Demir, Nucl. Phys. Proc. Suppl. **81** (2000) 224 [arXiv:hep-ph/9907279].
- [30] P. G. Harris *et al.*, Phys. Rev. Lett. **82** (1999) 904.
- [31] D. A. Demir and E. Ma, Phys. Rev. D **62** (2000) 111901 [arXiv:hep-ph/0004148].
- [32] D. A. Demir, E. Ma and U. Sarkar, J. Phys. G **26** (2000) L117 [arXiv:hep-ph/0005288].
- [33] D. A. Demir and E. Ma, J. Phys. G **27** (2001) L87 [arXiv:hep-ph/0101185].
- [34] R. D. Peccei and H. R. Quinn, Phys. Rev. Lett. **38** (1977) 1440.
- [35] J. E. Kim, Phys. Rev. Lett. **43** (1979) 103.
- [36] M. A. Shifman, A. I. Vainshtein and V. I. Zakharov, Nucl. Phys. B **166** (1980) 493.
- [37] M. Dine, W. Fischler and M. Srednicki, Phys. Lett. B **104** (1981) 199.

- [38] P Igo-Kemenes (2000) <http://www.cern.ch/LEPHIGGS/talks/index.html>.
- [39] M. Boz, Mod. Phys. Lett. A **17** (2002) 215 [arXiv:hep-ph/0008052].
- [40] S. Y. Choi and J. S. Lee, Phys. Rev. D **61** (2000) 111702 [arXiv:hep-ph/9909315].
- [41] S. Y. Choi and J. S. Lee, Phys. Rev. D **61** (2000) 115002 [arXiv:hep-ph/9910557].
- [42] S. Y. Choi and J. S. Lee, Phys. Rev. D **62** (2000) 036005 [arXiv:hep-ph/9912330].
- [43] A. Brignole, G. Degrassi, P. Slavich and F. Zwirner, Nucl. Phys. B **631** (2002) 195 [arXiv:hep-ph/0112177].